Controlled elastic postbuckling of bilaterally constrained non-prismatic columns: application to enhanced quasi-static energy harvesters

2016 Smart Mater. Struct. 25 125010

(http://iopscience.iop.org/0964-1726/25/12/125010)

IOP Publishing Smart Materials and Structures
Smart Mater. Struct. **25** (2016) 125010 (13pp) doi:10.1088/0964-1726/25/12/125010

Controlled elastic postbuckling of bilaterally constrained non-prismatic columns: application to enhanced quasi-static energy harvesters

Suihan Liu and Rigoberto Burgueño

Department of Mechanical Engineering, Michigan State University, East Lansing, MI, 48824, USA

E-mail: burgueno@msu.edu

Received 3 June 2016, revised 21 September 2016
Accepted for publication 13 October 2016
Published 10 November 2016

Abstract

Axially compressed bilaterally constrained columns, which can attain multiple snap-through buckling events in their elastic postbuckling response, can be used as energy concentrators and mechanical triggers to transform external quasi-static displacement input to local high-rate motions and excite vibration-based piezoelectric transducers for energy harvesting devices. However, the buckling location with highest kinetic energy release along the element, and where piezoelectric oscillators should be optimally placed, cannot be controlled or isolated due to the changing buckling configurations. This paper proposes the concept of stiffness variations along the column to gain control of the buckling location for optimal placement of piezoelectric transducers. Prototyped non-prismatic columns with piece-wise varying thickness were fabricated through 3D printing for experimental characterization and numerical simulations were conducted using the finite element method. A simple theoretical model was also developed based on the stationary potential energy principle for predicting the critical line contact segment that triggers snap-through events and the buckling morphologies as compression proceeds. Results confirm that non-prismatic column designs allow control of the buckling location in the elastic postbuckling regime. Compared to prismatic columns, non-prismatic designs can attain a concentrated kinetic energy release spot and a higher number of snap-buckling mode transitions under the same global strain. The direct relation between the column's dynamic response and the output voltage from piezoelectric oscillator transducers allows the tailorable postbuckling response of non-prismatic columns to be used as multi-stable energy concentrators with enhanced performance in micro-energy harvesters.

Keywords: stability, postbuckling, non-prismatic columns, energy harvesting

(Some figures may appear in colour only in the online journal)

1. Introduction

Harnessing the elastic buckling and postbuckling response of slender elements for use in smart/adaptive materials, devices and structures, rather than the traditional view as a failure state, has received much attention over the past decade with a wide range of applications such as sensors, actuators and energy harvesters [1, 2]. The major objective of energy harvesting is to generate electrical power by converting ambient vibrational energy [3] or thermal gradients [4], which provides various alternatives to power remote wireless sensors without the limitations of battery lifetime or wiring harnesses [5, 6]. One of the most common energy harvesting approaches is to use piezoelectric materials on vibration-based devices [4, 7]. This approach has a narrow range of frequency input for optimal performance, which has promoted

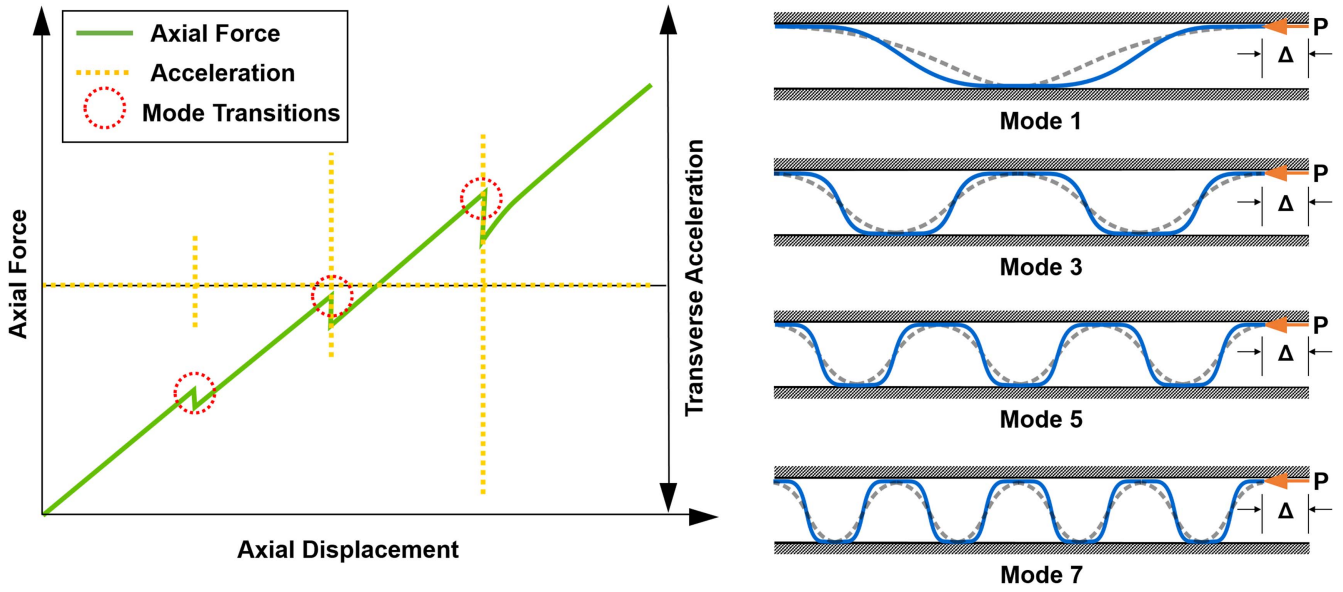

Figure 1. Schematic of key features in the elastic postbuckling response of an axially compressed bilaterally constrained column and the first few buckling modes, with profiles for point contact (dashed line) and line contact (solid line).

research and development of techniques to widen the operation frequency band of vibration-based energy harvesters. The new vision of harnessing structural instabilities has found its way towards the enhancement of energy harvesters by using the snap-through behavior of pre-buckled elements to introduce nonlinear behavior to linear generators, and thus overcome bandwidth limitations for higher efficiency. Jung and Yun [8] proposed an energy-harvesting device with buckled bridges to up-convert the generator's resonate frequency under low-frequency vibration excitation. An experimental investigation conducted by Sneller *et al* [9] showed that a post-buckled piezoelectric beam with attached central mass can achieve a broadened the frequency range over snap-through under a lower harmonic forcing amplitude. Enhanced power generations have also been found when thin piezoelectric beams are used in their buckled configuration under random vibrations [10] and chaotic vibrations [11]. Other attempts to expand the operational bandwidth of vibration harvesters include magnetic interactions [10, 12, 13], tunable resonators [14], amplitude limiters [15] and other concepts [7, 16]. However, even with a widened operational band frequency, all the previously noted harvesters are still limited to an external vibration input, and are thus inadequate for operating under quasi-static input sources. Low frequency deformation sources are very common in daily life, such as human walking motion and deformations in large civil structures [14]. Therefore, a new energy harvester concept was developed by our group that uses the multistable elastic buckling response of bilaterally constrained axially loaded beams/columns to allow harvesting energy from quasi-static ($\ll$1 Hz) input [15, 16]. However, the efficiency of the original design is limited due to the inability to control the postbuckling behavior of the bilaterally constrained column. Based on the original design, the concept of stiffness variations along the column is proposed in this paper to gain control of the buckling location for optimal placement of piezoelectric oscillators.

1.1. Postbuckling of bilaterally constrained columns

It is well established that multi-stable snap-through behavior in the elastic postbuckling regime of axially compressed slender columns can be obtained by the provision of bilateral rigid constrains (i.e., walls) to the transverse deformations of the element [17–19]. The sudden geometric transitions generated by this elastic unstable behavior have been demonstrated to be useful in transforming an external quasi-static displacement input into high-rate motions to excite vibration-based piezoelectric transducers for micro energy harvesting devices under very slow ($<$1 Hz) global input [20]. It follows that regulation of the noted postbuckling behavior can lead to controlled acceleration input to piezoelectric oscillators mounted on the slender element displaying the elastic instabilities and thus increased performance of the energy micro-harvester.

A homogeneous prismatic column with symmetric boundary conditions and subjected to an axial compressive load reaches its first critical stability point and buckles with a maximum transverse deformation amplitude at mid-span. If the column is provided with continuous rigid parallel lateral supports, a contact zone develops between the element and the constraints, which grows from a condition of point contact to line contact with increasing load [17]. The first few buckling modes for the case in which the axially loaded column is initially placed adjacent to one of the constraining walls are shown in figure 1, which shows the transition from point to line contact for the different buckling modes. After a line contact condition has developed, the bending moment vanishes within this region due to the lack of curvature and independent boundary conditions form for the segment,

equivalent to clamped–clamped ends in an Euler column, develop. Local snap-through-type buckling occurs in the longest flattened region when the critical load within this segment is reached [17, 18, 21]. The higher order buckled configuration forms after the snap-through event corresponds to a lower state of energy. The released strain energy transforms to kinetic energy and induces a transverse acceleration impulse on the strip at the locations of contact with the constraining walls.

Key features in the postbuckling force-deformation response of an axially-compressed column are showcased in figure 1. The snap-through buckling events, or mode transitions, are reflected as load drops on the displacement-controlled force-deformation response trace, and as acceleration impulses at the same time instances [20]. The acceleration impulses are due to the local bifurcations, which are sensitive to their location along the column. A small local motion may generate a large acceleration at that location but it could correspond to a relatively small global kinetic energy release. Therefore, controlling the location of local buckling events can help to strategically place piezoelectric oscillators for the purpose of optimizing pseudo-static micro-energy harvesting devices.

1.2. Limitations on controlling bilaterally constrained uniform columns

For an axially compressed column exhibiting an elastic postbuckling response the equilibrium shape is determined by a balance of the column's bending and compressive energy with the energy from the external applied force. For a bilaterally constrained column, the shape during the deformation process is divided into flat and curved segments once line contact has formed (figure 1). The key parameter triggering the buckling mode transitions is the length of the isolated line contact sections [17, 21]. Assuming that the total length of flat segments remains constant, thus keeping the total strain energy is unchanged, different buckled equilibrium shapes can be formed by redistribution of the flat segments along the column [21]. The buckled shapes for modes 1 and 3 are shown in figure 2, where the line contact regions are indicated as segments a, b and c. The deformed profile to accommodate the end shorting ΔL is assumed symmetric [17, 18], where $2a = 2b = c$. However, the buckling shapes are typically asymmetric due to friction between the column and the side walls. This asymmetry, first noticed by Chai [17, 18] and then others [21, 22], affects the distribution of line contact segments. Based on Euler's buckling equation the critical buckling load is inversely proportional to the critical length [23]; that is, the longer the column the easier it is for it to buckle. Thus, upper and lower limits can be considered for the generation of mode transitions. In the upper limit, the condition that $a = b = c$ requires the straight segments to be as short as possible, which makes instability more difficult. In the lower limit $a = b = 0$, thus making segment c the longest. For the purpose of this study it is desired that the column behaves like the lower limit case to achieve the highest number of local instabilities.

The generation of mode transitions is bounded within the noted limits but the buckling location in a uniform strip varies and cannot be isolated due to the changing buckling configurations after each mode transition, the effects of initial imperfections, alignment of the strip with respect to the constraining walls, and friction between the strip and the constraints. This makes location and sequence of the buckling events uncontrollable for optimal placement of piezoelectric harvesters.

1.3. Motivation and hypothesis

The column configuration (i.e., deformed shape, or elastica) between the constraining walls is the one that accommodates the end shortening with the minimum potential energy. The hypothesis behind this study is that the energetically favorable (lower) configuration is achieved by reducing the bending strain energy from stiff regions by introducing stiffness variations along the column length. The larger bending resistance of stiff segments will allow them to remain straight and develop a line contact with the constraints while flexible regions accommodate the end shortening primarily through bending. Therefore: (a) a higher number of local instabilities and (b) controlled (or predefined) buckling locations can be achieved. Non-prismatic columns with stiffness variations were thus considered based on the lower limit buckling configuration and schematics are shown in figure 2 for buckling modes 1 and 3.

Studies related to the stability of non-uniform columns and the advantage that they could offer for controlling static and dynamic response date back to more than a century. However, most efforts have focused on determining the critical buckling load of non-uniform beams/columns/rods subject to varying axial loads and boundary conditions with [24, 25] or without laterally restraints [26–29] through closed-form solutions, and also via a semi-analytical procedures [30] and higher-order perturbation approach [14]. Details on these solutions can be found in reference [31]. Use of non-uniform strip elements for controlling static and dynamic response by strategic selection of non-uniform cross-section geometry and materials has also been explored [32, 33]. However, the studies conducted thus far focus on the onset of buckling and up to the first bifurcation in the postbuckling response. Yet, a recent related study by our group [34] has shown that the elastic postbuckling response of cylindrical shells can be tailored by introducing non-uniform stiffness distributions. It follows that the multi-stable response non-prismatic columns in the far elastic postbuckling regime remains unexplored and that non-prismatic column design is a viable way to tailor the desired elastic instabilities.

1.4. Dynamic features for use in energy harvesting devices

The acceleration impulses generated by the postbuckling mode transitions of the bilaterally constrained column act as a transverse base input excitation to a piezoelectric energy harvesting transducer (cantilever bimorph) to generate voltage output. The piezoelectric oscillator is attached to the slender

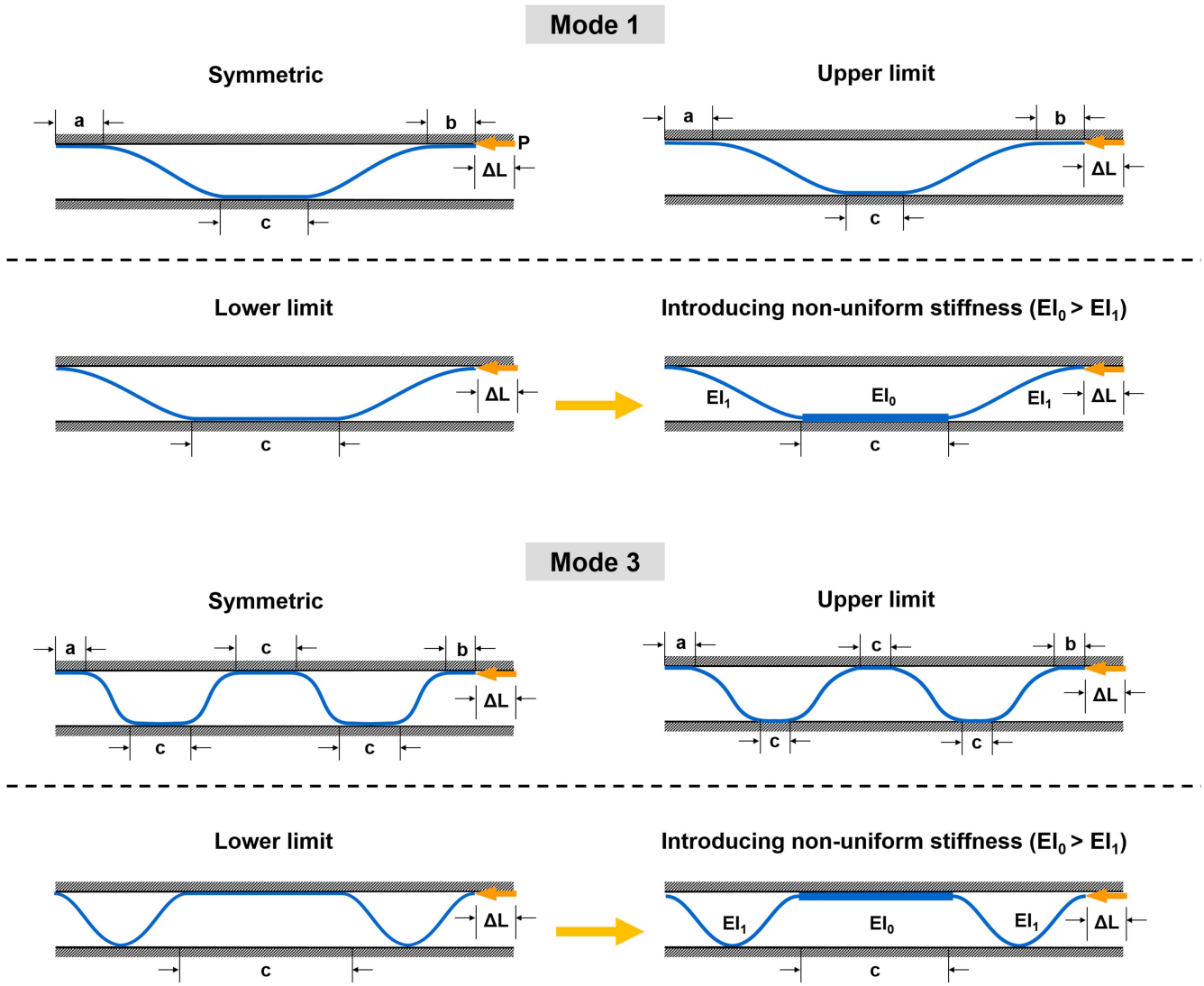

Figure 2. Schematic depiction of different buckling shapes for modes 1 and 3: symmetric case, upper and lower limit cases, and the effect of non-uniform stiffness on the buckling shapes.

axially loaded column element (with the cantilever's longitudinal axis perpendicular to the supporting column's own longitudinal axis so that it responds as a single-degree-of-freedom oscillator (figure 5(b)). The correlation between the base acceleration input (resulting from the snap-buckling events of the axially loaded bilaterally constrained column) and the generated piezoelectric voltage output from a bimorph PVDF cantilever with properties shown in table 1 is illustrated with simulated results in figure 3. The acceleration impulses have positive and negative magnitudes (directions normal to the strip's surface) as a result of the column's wall impact and reaction directions [20]. Therefore, a synthetic acceleration record (figure 3(a)) with impulses of varying magnitudes: equal values in both directions (1–3 s), larger value in the positive direction (4–6 s) and larger value in the negative direction (7–9 s) was designed to represent different scenarios in the dynamic response of a bilaterally constrained strip during elastic postbuckling. The acceleration record was then used as the base excitation for the bimorph piezoelectric cantilever beam and the generated voltage output calculated using a simplified Rayleigh–Ritz approach [35] is shown in figure 3(b). As expected, the generated voltage clearly corresponds to the acceleration pulses. It can also be seen that the magnitude of the output voltage is directly proportional to the

Table 1. Properties of the piezoelectric oscillator.

Property	Value (piezoelectric PVDF/substrate)
Young's modulus	2 GPa/2.4 GPa
Density	1780 kg m^{-3}/1390 kg m^{-3}
Thickness	28 μm/205 μm
Width	12 mm/16 mm
Length	27 mm
Tip mass	3.15 g
Piezo strain constant d_{31}	23×10^{-12} C N^{-1}
Piezo strain constant d_{33}	-33×10^{-12} C N^{-1}
Piezo stress constant g_{31}	216×10^{-3} Vm N^{-1}
Piezo stress constant g_{33}	-330×10^{-3} Vm N^{-1}
Electrical permittivity	115 × 10-12 F m^{-1}
Capacitance	280 pF cm^{-2} @ 1 KHz

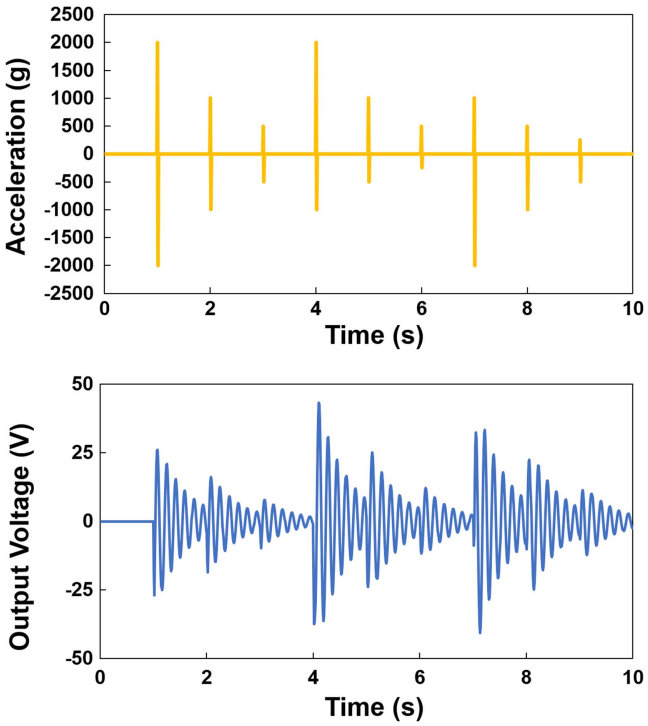

Figure 3. Piezoelectric voltage output by a bimorph piezoelectric oscillator from a set of acceleration impulses.

magnitude of the acceleration impulse. Therefore, enhanced performance of the energy harvesting device, from the system's mechanical aspect, requires that the targets for the elastic postbuckling behavior of the strip be: (a) increasing the number of acceleration impulses or mode transitions, (b) increasing the magnitude of the accelerations impulses, and (c) controlling (or predetermining) the buckling locations. The results of this study are evaluated in later sections under these parameters. It is recognized that energy harvesting can also be enhanced by modifying the piezoelectric oscillator, but such an approach is beyond the scope of this study.

2. Methods

2.1. Non-prismatic column/strip designs

Stiffness variation within a column was introduced by changing its thickness, which is the most effective parameter to control bending stiffness along segments of its length. Column designs with thickness variations in three segments along their length were considered (see figure 4) based on the configuration of the lower buckling limits (see figure 2). The segment distribution with respect to the column's length was symmetric. The geometry and material properties of the baseline uniform column are given in table 2. The middle (thicker) segment thickness, t_0, for all non-prismatic designs was equal to the uniform thickness in the baseline column. The ratio between the outer (thinner) segment thickness t_1 and the baseline column thickness was defined as $\alpha = t_1/t_0$; and the ratio between the thicker segment length to the column length L_0 was defined as β. The value of β was limited as $0.25 \leqslant \beta \leqslant 0.65$ to avoid extreme values towards a prismatic column. The dimensionless parameters α and β were varied to generate different designs. The postbuckling behavior of non-prismatic columns with different combinations of α and β was experimentally and numerically investigated, and further analyzed by a theoretical model. The results were also compared with those from the baseline (prismatic) column.

2.2. Experimental evaluations

Following the proposed non-prismatic column design, five non-prismatic columns and the prismatic baseline column were tested. The test strips (figure 5(a)) were fabricated with a 3D printer (Objet Connex350, Stratasys Ltd, Eden Prairie, MN) using a rigid photo-polymer material (VeroWhite RGD835). The rigid constraints in the test setup consisted of aluminum plates (figure 5(b)). The walls were separated by a gap h_0, such that the h_0/t_0 ratio was kept constant at 1.7 to keep consistency with our previous work [20]. The strip was fully fixed at the bottom, and rotations and transverse translations were constrained at the top. The strip was subjected to a full loading and unloading cycle (20 s period) of axial compression under controlled end shortening to a target of 3.8 mm (i.e., 2% global axial strain).

A PVDF piezoelectric energy-harvesting oscillator (properties given in table 1) was mounted in a cantilever configuration at the mid-span of both prismatic and non-prismatic columns to compare the harvested energy levels. The voltage generated by the PVDF beam was measured using an oscilloscope (RIGOL DS1102E, China) with a 100 MΩ resistor connected in parallel. Considering the mass and beam length of the PVDF film the bilaterally constrained column setup transforms the input deformation frequency from 0.05 Hz (20 s loading/unloading cycle period) to the harvester's natural frequency of 5.85 Hz.

2.3. Theoretical analysis

A theoretical model is developed as shown in figure 6 to predict the critical line contact section length, mode transitions and the buckling shapes of the proposed non-prismatic columns with fixed–fixed boundary conditions under controlled end shortening in the bilaterally constrained setup. The model is based on the results of Chai [17, 18] and the simplified approach of Xiao and Chen [21] for uniform columns. Figure 6(a) presents the undeformed column with two equal-length outer segments with flexural stiffness $EI_1 = Ebt_1^3/12$ and cross-sectional area $A_1 = bt_1$, and a middle segment with flexural stiffness $EI_0 = Ebt_0^3/12$ and cross-sectional area $A_0 = bt_0$. The other parameters follow the descriptions in section 2.2 and contact friction is neglected. Under the assumption that the column stays at the lower limit configurations (figure 2), the first three buckling modes are as presented in figures 6(a)–(d), where the straight section only appear at the middle region of the column. The deformed shapes consist three parts [17, 18, 21]: the curved sections with projected length L_2, the straight section L_1, and the end

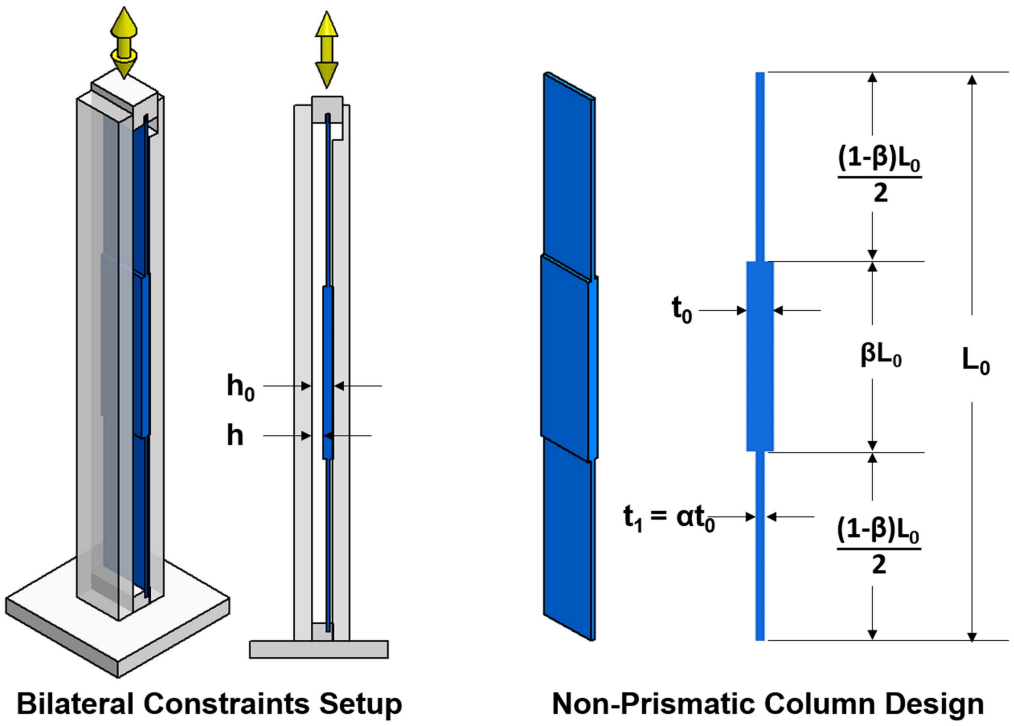

Figure 4. Non-prismatic column design concepts.

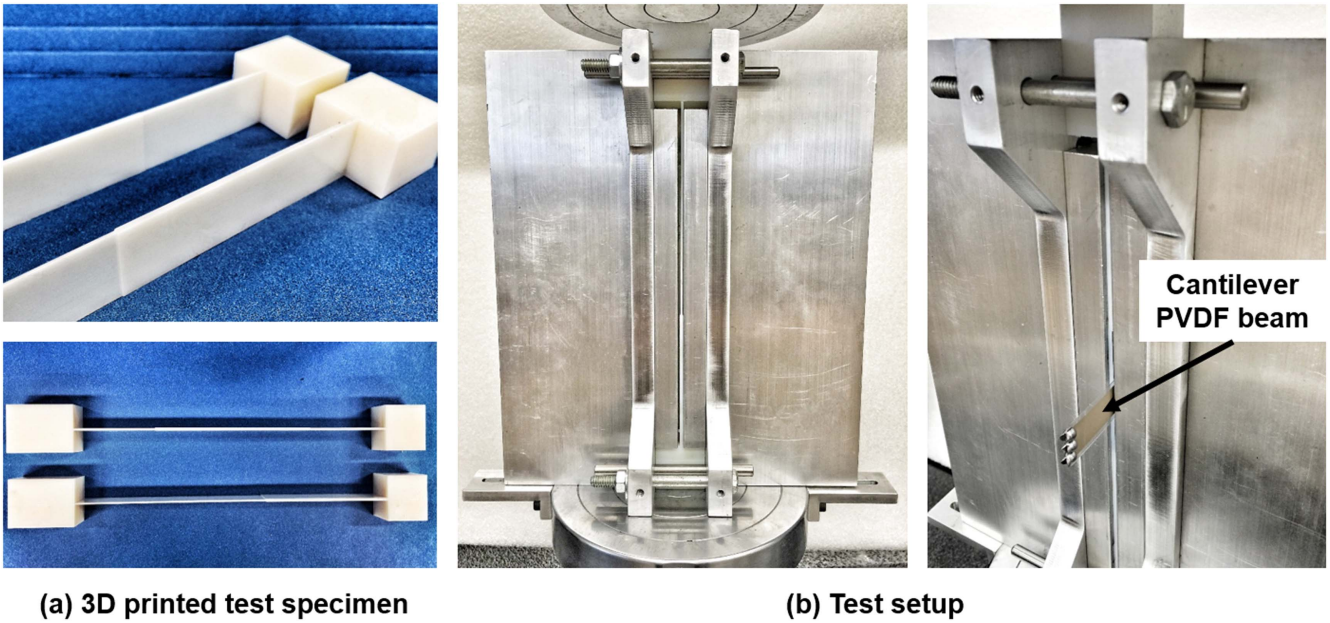

Figure 5. Experimental evaluation: (a) view of a 3D printed strip test specimen and (b) test setup.

Table 2. Geometry and material properties of the baseline column.

Property	Value
Elastic modulus, E	2.5 GPa
Column length, L_0	190 mm
Width, b	20 mm
Thickness of base column, t_0	1.78 mm

shortening ΔL; which yield the column's total length $L_0 = \Sigma L_2 + L_1 + \Delta L$. An elastic Euler beam under axial compression can be expressed as a fourth-order linearized differential equation [17, 27] as:

$$y'''' + k^2 y'' = 0,\ k^2 \equiv \frac{P}{EI_i}, \tag{1}$$

where P and I_i are the compression force and the moment of inertia of the segment, respectively. Taking mode 1 as an example, the shape of the curved sections between $x = [0, L_2]$

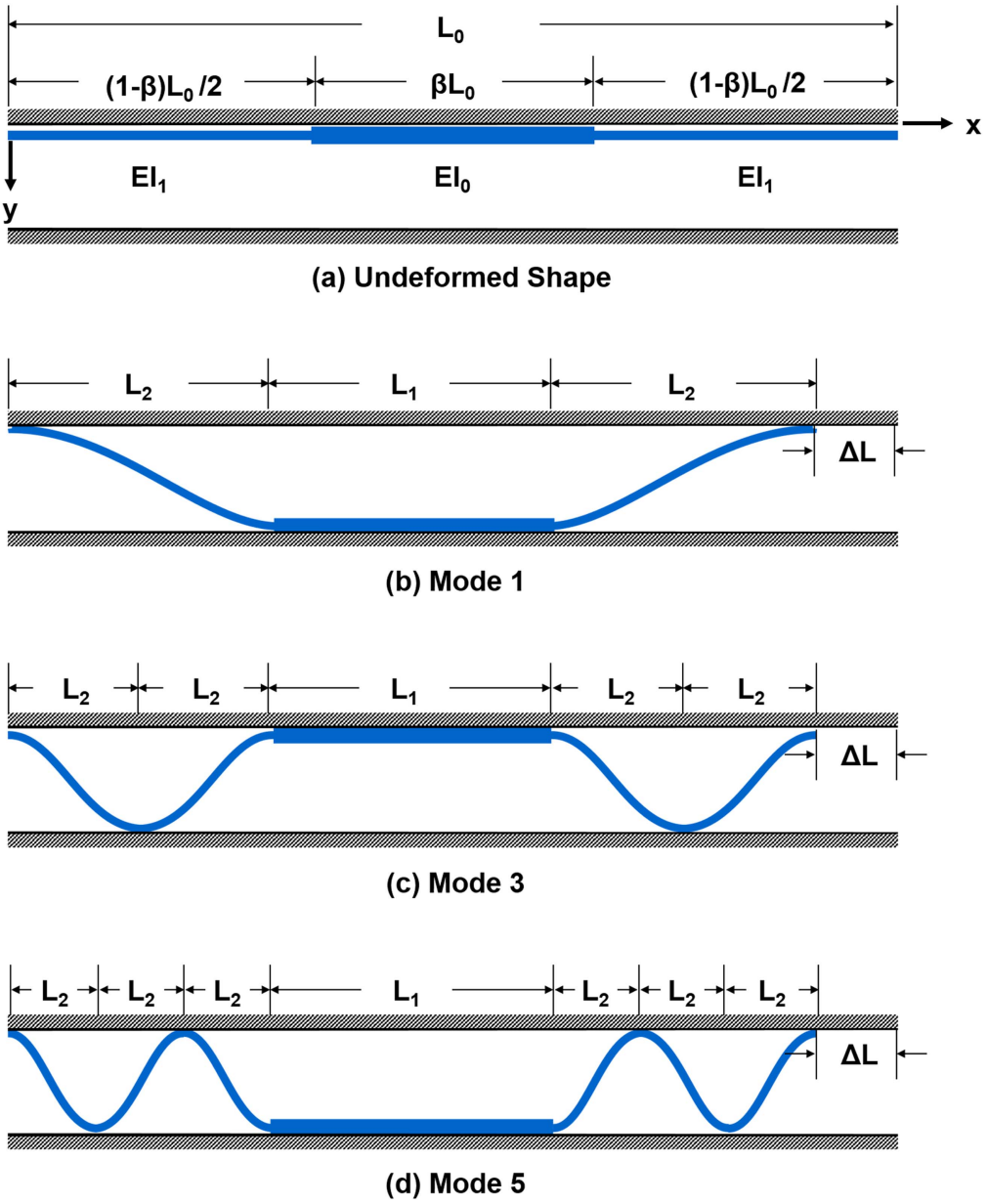

Figure 6. Schematic of the theoretical model with the first three buckling mode configurations.

and $x = [L_1 + L_2,\ L_1 + 2L_2]$ can be written as in equations (2) and (3):

$$y = \frac{h_0}{L_2}x - \frac{h_0}{2\pi}\sin\left(\frac{2\pi}{L_2}x\right), \tag{2}$$

$$y = -\frac{h_0}{L_2}(x - L_1 - 2L_2) + \frac{h_0}{2\pi}\sin\left(\frac{2\pi}{L_2}(x - L_1 - 2L_2)\right), \tag{3}$$

where h_0 is the gap between the constraining walls. The constraint of coefficient k in equation (1) satisfies $kL_2/2\pi = 1$. The buckling shapes are consistent with finite-element simulation results, and the shape of the curved sections in other modes can be represented in a similar manner. Therefore, the length of the curved sections can be calculated as:

$$L_{\text{curved}} = \sum\int_L \sqrt{1 + (y')^2}\,\mathrm{d}x. \tag{4}$$

The total length of the deformed column is $L_{\text{deformed}} = L_{\text{curved}} + L_1$. The linear axial strain is

$$\varepsilon = \frac{L_{\text{deformed}} - L_0}{L_0}. \tag{5}$$

The potential energy of the column in this model is considered to consist two parts: compression energy and bending energy. The compression energy is assumed to be uniform per cross-sectional area along the column and the bending energy is assumed to only exist in the curved sections

[21]. Therefore, the compression energy of the column is

$$E_{\text{compression}} = \frac{E\varepsilon^2}{2}(A_0\beta L_{\text{deformed}} + A_1(1-\beta)L_{\text{deformed}}). \quad (6)$$

The bending energy of the curved sections when $L_{\text{curved}} \leqslant (1-\beta)\, L_{\text{deformed}}$ is

$$E_{\text{bending}} = \frac{EI_1}{2}\int_L \frac{(y'')^2}{(1+y'^2)^3}\mathrm{d}x \quad (7)$$

and when $L_{\text{curved}} > (1-\beta)\, L_{\text{deformed}}$ is

$$E_{\text{bending}} = \frac{E}{2}\left[\left(\frac{L_{\text{curved}}}{L_{\text{deformed}}} - 1 + \beta\right)I_0 + \left(\beta - \frac{L_{\text{curved}}}{L_{\text{deformed}}}\right)I_1\right]\int_L \frac{(y'')^2}{(1+y'^2)^3}\mathrm{d}x. \quad (8)$$

Therefore, for a given end shortening ΔL, either the length of the straight section length L_1 or the length of the curved section L_2 can be determined at the minimum potential energy (i.e., $E_{\text{compression}} + E_{\text{bending}}$). Thus, the buckling shape configurations can be estimated accordingly.

The critical strain of the straight section L_1 is calculated as

$$\varepsilon_{\text{cr}} = \frac{\pi^2 E}{\left(\frac{KL_1}{\text{r}}\right)^2},\ r = \frac{1}{A_0^2}. \quad (9)$$

However, the effective length factor, K, is uncertain since the boundary conditions of the straight section L_1 are somewhere between pin–pin ($K = 1$) and fixed–fixed ($K = 0.5$). The average value of $K = 0.75$ is adopted here. Therefore, the column buckles under a certain end shortening when the following two criteria are both satisfied: the compressive strain exceeds the critical strain at L_1 and the minimum potential energy is lower at the next higher buckling mode configuration.

2.4. Numerical simulations

Numerical simulations were conducted using the finite element program ABAQUS (Simulia 2014). The column was modeled with four-node quadrilateral finite-membrane-strain elements (S4). The analysis procedure followed two general steps: a linear eigenvalue analysis of the ideal column and a second-order elastic dynamic analysis of the column with artificial imperfections. In the linear analysis, the critical buckling loads and the corresponding mode shapes are found. The dynamic analysis was conducted using the implicit solver in ABAQUS with consideration of large deformations. An artificial imperfection based on the superposition of buckling mode shapes was added to the column's original geometry to trigger the second-order effects. The seeded imperfection had contributions from four mode shapes with gradually decreasing amplitude with respect to the column's thickness: 1st (3%), 3rd (0.23%), 5th (0.08%) and 7th (0.016%). Consistent with the experimental setup (section 2.2) the column/strip in the model was placed so that it was adjacent to one of the constraining walls. Since shell elements have no physical thickness, the distance between the rigid walls and the strip was the net gap $h = h_0 - t_0$. An offset of 5% of the net gap was provided on the near wall side to accommodate the seeding of initial imperfections for the nonlinear analysis and to avoid interaction with the no penetration rigid wall boundary and the strip. The constraints were modeled with rigid shell elements with no-penetration contact behavior. The friction coefficient between the wall and the column surfaces was 0.2, chosen by calibration of the simulation results with test data.

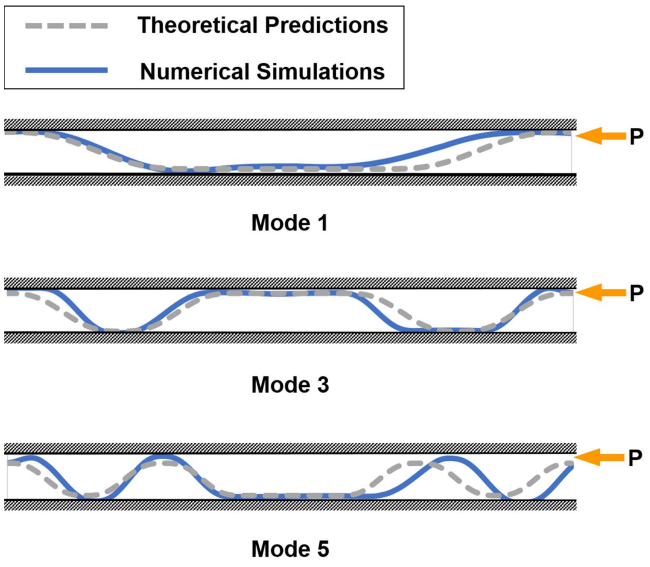

Figure 7. Comparison between the theoretical predictions and numerical simulations of the critical buckling configurations for the first three modes. The gap is scaled 3 times for clarity.

3. Model validations

3.1. Theoretical model versus numerical simulation

The theoretical predictions and numerical simulations of the critical buckling configurations (i.e., buckling shapes right before mode transitions) of the first three modes for a non-prismatic column ($\alpha = 0.80/\beta = 0.35$) are compared in figure 7. It can be seen that the models are in good agreement on predicting the critical straight section length, which is the key for triggering mode transitions. Larger discrepancies are found at the two outer curved sections that are mainly caused by three reasons. First, the buckling shapes in the theoretical model assumed that the flat segment only formed at the middle of the column. However, this ideal lower limit configuration cannot be achieved in reality. A more detailed description with experimental results is presented in section 4.1. Second, the contact friction, which is neglected in the theoretical model, causes asymmetry on the buckling shapes of the numerical simulations. Third, using small deformation theory and linear strain lead inaccuracies in the theoretical analysis when the buckling wave number and curvature increases [17, 18]. In spite of the noted

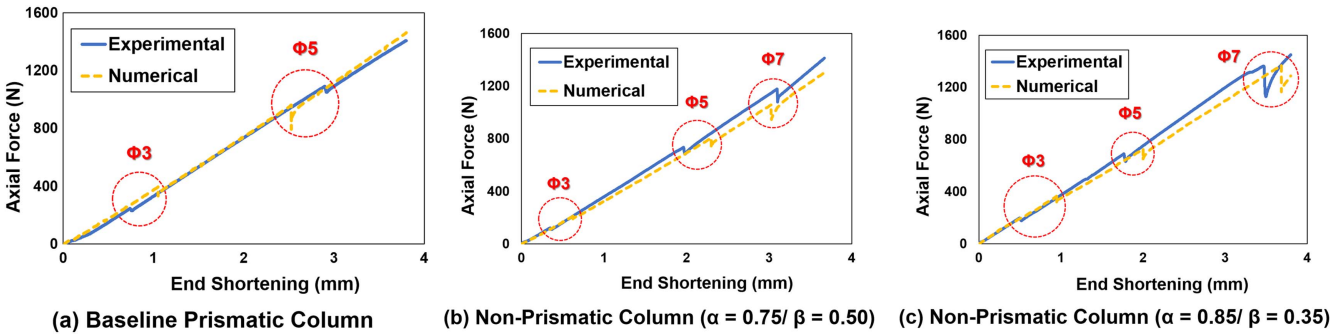

Figure 8. Comparison of experimental and numerical force–displacement responses of the prismatic baseline column and two non-prismatic columns.

shortcomings, the theoretical model is considered to provide an adequate prediction of the buckling morphologies and it is adopted to study the effect of the critical straight segment length on the column's local instabilities.

3.2. Numerical simulation versus experimental results

Experimental and simulation results for the first two mode transitions are summarized in table 3. The force–displacement responses of the baseline and two non-prismatic design cases ($[\alpha/\beta] = [0.85/0.35]$ and $[0.75/0.50]$) are presented in figure 8. The snap-through events for each buckling mode transition are circled. It can be seen that the FE simulations adequately captured the mode transitions and the initial and end response stiffness. The differences between the simulated and experimental responses are due to uncertainty in modeling parameters, such as the actual imperfections, friction resistance between and strip and walls, and the boundary conditions. Nonetheless, the simulation approach is considered acceptable for the purpose of this study given that the simulations can adequately capture the number and onset of the mode transitions, the initial and end stiffness, and the magnitude of the load drops.

It should be noted that while the presented research is motivated by the development of micro-energy harvesters, the study was performed on meso-scale prototypes and not a final packaged device. The meso-scale investigation is appropriate to evaluate the mechanics aspects of the energy concentrator (axially compressed column) and triggering (snap-buckling) since unstable elastic response has been proven to be scale invariant [36]. Thus, the reported force and deformation levels are to be considered for comparison with samples of the same study and not in absolute terms as those required in a deployable device. Deployment of the concept into actual devices will have to be scaled accordingly depending the application and the force and deformation levels required to trigger the buckling events will also change.

4. Results

4.1. Controlled local buckling location and increased level of instabilities

The experimental configurations for each mode transition of the baseline column and a non-prismatic column ($\alpha = 0.85/\beta = 0.35$) during the loading phase are shown in figure 9. The line contact regions before each mode transition are also indicated in the figure. It can be observed that for both columns the snap-through events are always generated at the longest line contact region (shown by the red arrows). Thus, controlling the formation of the longest line contact region allows control of the buckling locations. The length of the straight segment increases with axial shortening. In the prismatic column there is no control of the buckling location since the distribution of the line contact segments changes as the mode configuration shifts. However, the longest straight segment is always located in the middle of the non-prismatic column (figure 9(b)) due to its larger bending resistance. This allows it to behave similar to the lower limit case proposed in

Table 3. Comparison of simulation and experimental postbuckling results.

Case		Mode 3						Mode 5					
		Disp. (mm)			Force (N)			Disp. (mm)			Force (N)		
α	β	Exp.	Num.	Diff.	Exp.	Num.	Diff.	Exp.	Num.	Diff.	Exp.	Num.	Diff.
0.7	0.4	1.1	1.2	0.1	285.0	312.0	27.0	2.5	2.6	0.2	667.5	691.0	23.5
0.75	0.5	0.4	0.6	0.3	117.1	203.9	86.8	1.9	2.2	0.3	595.0	614.0	19.0
0.8	0.45	1.2	1.2	0.0	338.0	412.0	74.0	1.8	1.9	0.1	589.0	606.0	17.0
0.85	0.35	0.4	0.6	0.3	117.1	193.3	76.2	2.0	2.3	0.4	734.5	799.8	65.3
0.9	0.5	0.6	0.8	0.2	256.0	309.0	53.0	3.0	2.5	0.5	1216.0	1036.0	180.0
Baseline		0.7	1.1	0.4	271.9	375.3	103.4	2.9	2.5	0.4	1083.1	961.7	121.4

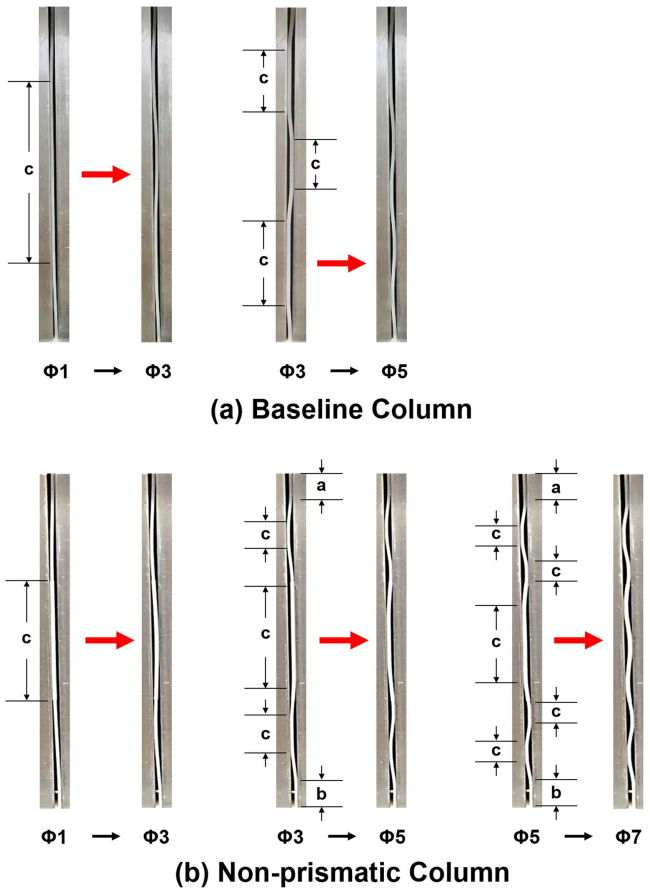

Figure 9. Post-buckling transition process as obtained from experiments for (a) baseline design and (b) non-prismatic design case $\alpha = 0.85/\beta = 0.35$.

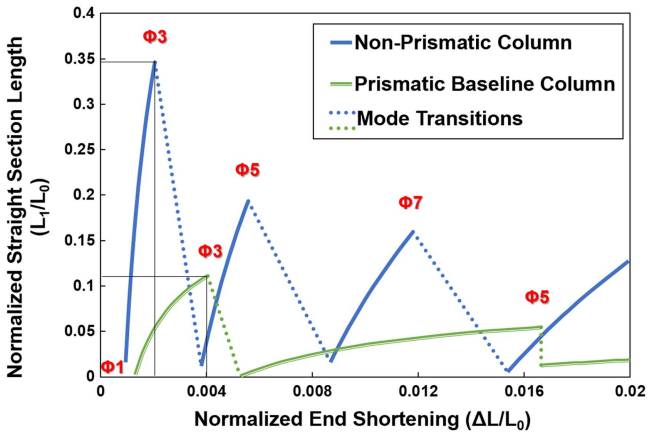

Figure 10. Development of the middle straight section length versus column end shortening from theoretical analysis (the data is normalized by the column length L_0) for the baseline design and non-prismatic design case $\alpha = 0.85/\beta = 0.35$.

figure 2. The mode shapes of the non-prismatic strips also feature localized transverse deformations in the flexible segments that are superposed on the global buckling shape. This is due to the distribution of transverse deformations from traveling strain energy stress waves from the stiffer regions to the flexible ones after the snap-through mode transitions.

Figure 10 compares the change in length of the straight segment as a function of end shortening to a maximum of 2% strain for the baseline and non-prismatic ($\alpha = 0.85/\beta = 0.35$) columns, the results are from the theoretical model (section 2.3) and normalized by the column length L_0. For both cases, at the pre-buckling stage the length of the straight section is clearly zero as end shortening increases until the column buckles and teaches one side of the walls. The line contact region keeps growing as compression proceeds and is followed by a downward jump upon reaching the critical point. The columns then re-stabilize at a higher buckling mode configuration until the next buckling limit is reached. The solid lines indicate the stable states during the post-buckling process and the dotted lines indicate the unstable mode transition phases. It can be seen that for the non-prismatic column the normalized critical straight section length at the transition to mode 3 is 0.35 (i.e., the same as β). This corresponds to the experimental results shown in figure 9 where all of the middle segment length was in contact with the wall before buckling. As the buckling mode increases, the line contact regions reduce in length to accommodate the increased number of buckling waves in the outer segments and the end shortening (figure 9). Therefore, the middle straight section gets shorter each time the column jumps to a higher mode; which requires a larger end shortening to trigger the next buckling event, as shown in figure 10.

Taking the transition to mode 3 as an example, the results in figure 10 show that the non-prismatic column forms the straight line contact section quicker and reaches the critical limit sooner compared to the prismatic baseline column. This comparison holds true for every mode transitions shown, as a much steeper slope of the curves representing the straight section length development with end shortening for the non-prismatic column. Therefore, in addition to permitting control of the buckling location, the non-prismatic design accelerates the development of local instabilities and is able to attain a higher number of buckling mode transitions under the same global deformation level (2% global axial strain) compared to the baseline uniform design.

The evolution of buckling shapes (i.e., normalized transverse deflection with respect to the gap distance h_0 of the strip) for each mode transition of the non-prismatic case ($\alpha = 0.85/\beta = 0.35$) from the FE simulations is shown in figure 11. The predicted buckling shapes and the mode transitions are consistent with the experimental results in that every snap-through event is triggered at the middle thicker segment. Besides allowing control of the buckling location, stiffness variations along the column lead to a transient response after mode transitions that is quite different to that in prismatic columns. In the postbuckling response of a uniform strip the new mode shape stabilizes quickly after the snap-through buckling event and the column's deformed shape experiences minor changes until the next mode jump occurs. However, non-prismatic strips display a longer transient dynamic response following snap-through buckling events and stress waves travel along the strip leading to the propagation of local buckling deformations within the global stable

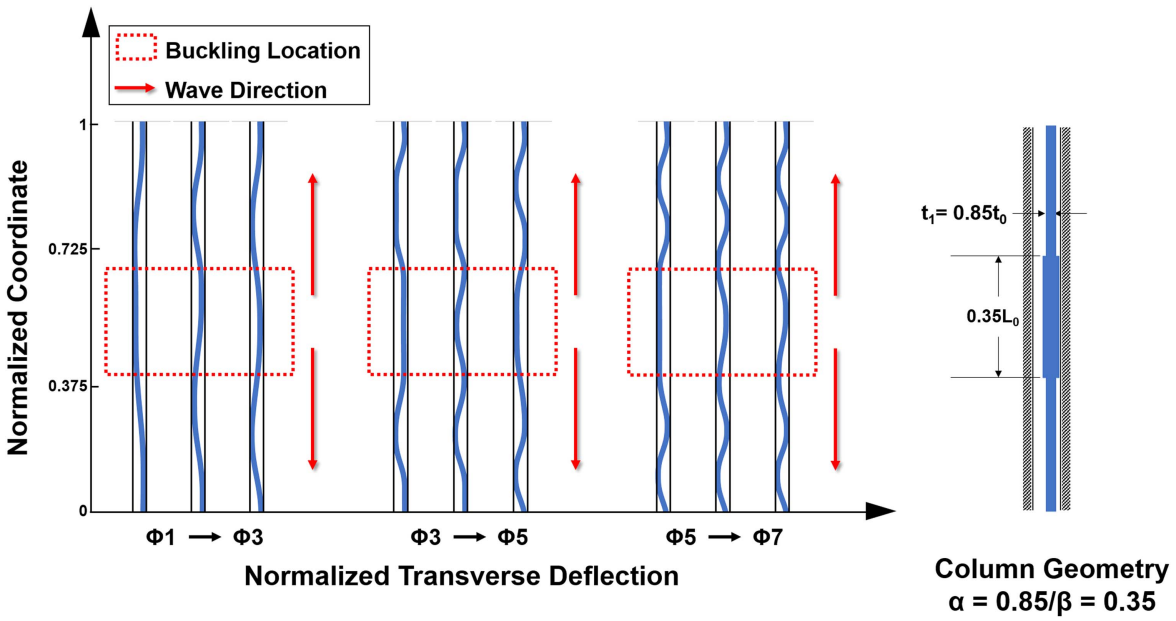

Figure 11. Post-buckling transition process as obtained from finite element simulations for non-prismatic design case $\alpha = 0.85/\beta = 0.35$ (the longitudinal coordinate is normalized by the column length L_0; the transverse deflection is normalized by the gap distance h_0).

Table 4. Comparison of the absolute maximum acceleration, average acceleration of all impulses and the number of impulses at the mid-span of the thicker segment (controlled buckling location) and thinner segments for selected cases.

Cases		Abs. max. acc. (10^3 g)			Avg. acc. (10^3 g)			No. of acc. impulses		
α	β	Outer seg.	Middle seg.	% Diff.	Outer seg.	Middle seg.	% Diff.	Outer seg.	Middle seg.	Diff.
0.80	0.35	2.35	3.7	36.5	1.32	2.03	35.0	3	3	0
0.80	0.50	1.27	3.63	65.0	0.76	1.98	61.7	3	2	1
0.85	0.35	3.76	13.5	72.2	2.95	8.88	66.7	4	3	1
0.90	0.45	0.84	8.2	89.8	0.11	4.33	97.4	4	2	2
0.90	0.35	8.02	9.85	18.6	3.59	8.00	55.1	3	3	0

buckling shape. Once the stiffer region buckles, a relatively larger deformation and curvature develops at the stiffer region compared to the rest of the column. However, the stored strain energy seeks minimization in its distribution along the strip and propagates to the thinner regions, which have lower bending stiffness, finally stabilizing at the lowest potential energy level. The wave's traveling direction is shown with arrows in figure 11.

It is also of interest to compare the postbuckling response features of different segments in the non-prismatic columns. The maximum acceleration, average acceleration and the number of acceleration impulses at the mid-span of each segment in the column are compared in table 4 for five selected non-prismatic designs. The value shown for the outer segment is the average from the upper and lower thin segments. It can be seen that both the maximum and average acceleration at the controlled buckling location (thicker region) are significantly higher. This is attributed to a relatively larger mass and kinetic energy release at the middle thicker segment, where the buckling-induced high rate motions were generated. Regarding the number of acceleration impulses: in most cases more events were found at the outer segments; a response feature that is due to the propagation of stress waves towards these regions, which experience local motions in addition to the global mode transitions.

4.2. Response map

Experimental observations showed that when α was less than 0.7 the thicker segment would not be able to buckle due to insufficient force transfer from the thin segment and a kink was observed at the stiffness interface of the strip for the three segment case with $\alpha = 0.5$ during loading. When α was greater than 0.90 there was insufficient stiffness variation between segments to make the non-prismatic column behave differently from a prismatic one. Thus, the range of α was selected to be $0.7 \leqslant \alpha \leqslant 0.9$. Forty-five cases of non-prismatic columns were numerically studied within this domain and results are shown in figure 12 as a response map for the non-prismatic column design. The postbuckling response was evaluated by two parameters: the highest buckling mode shape reached and whether the buckling location was controlled (i.e., pre-determined) or un-controlled. The design domains with controlled buckling location are enclosed by the hatched region in the diagram. This result supports the

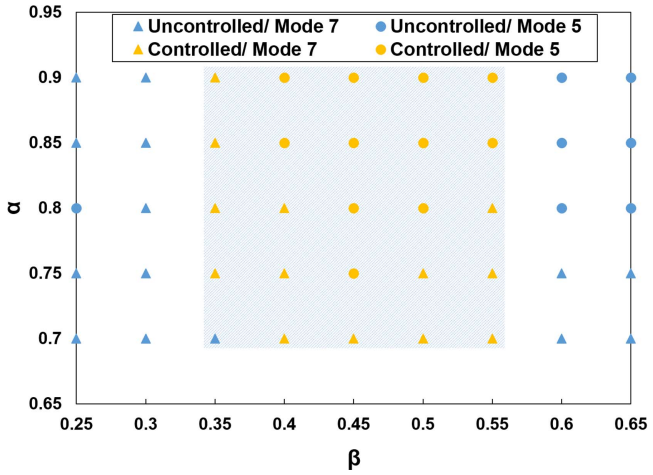

Figure 12. Effect of α and β on the postbuckling location and highest achievable buckling mode for the non-prismatic column design. Hatched regions are design domains with controlled buckling response.

hypothesis that buckling location along the element can be contolled at the stiff segments by reducing the bending strain energy from these regions that allow them to remain straight and develop a line contact with the constraints, therefore dictating the triggering location of the snap-through buckling events. Limits to the influence of non-prismatic designs for controlled postbuckling response can also be identified in figure 12 when the thickness and length ratios between segments reach extreme values. The response map thus provides guidance for designing non-prismatic column elements as energy concentrators to excite vibration-based piezoelectric transducers.

4.3. Enhanced energy generation

Figure 13 presents, from experiments, the applied axial force and the output piezoelectric voltage of a PVDF oscillator transducer (table 1) attached to a prismatic baseline column and a non-prismatic column ($\alpha = 0.80/\beta = 0.40$) in the configuration shown in figure 5(b), for a full loading/unloading 20 s cycle. It can be clearly seen that the non-prismatic column generated a higher level and more sustainable voltage output. Since the buckling location is uncontrolable in the prismatic column, the local buckling motions are not always at the mounting location of the harvester (column mid-height) for every mode, which leads to a much lower level of harvested power. Compared with the baseline column, the increased number global mode transitions of the non-prismatic column provides a more continous series of acceleration impulses to the oscillator, and the predefined buckling location at the column mid-height allows all the mode transitions to transmit larger levels of acceleration input to the PVDF oscillator. Therefore, enhanced performance of the energy harvesting device was achieved by controlling the elastic postbuckling behavior of the non-prismatic strip with increased/enlarged acceleration impulses and a predefined and concentrated buckling location.

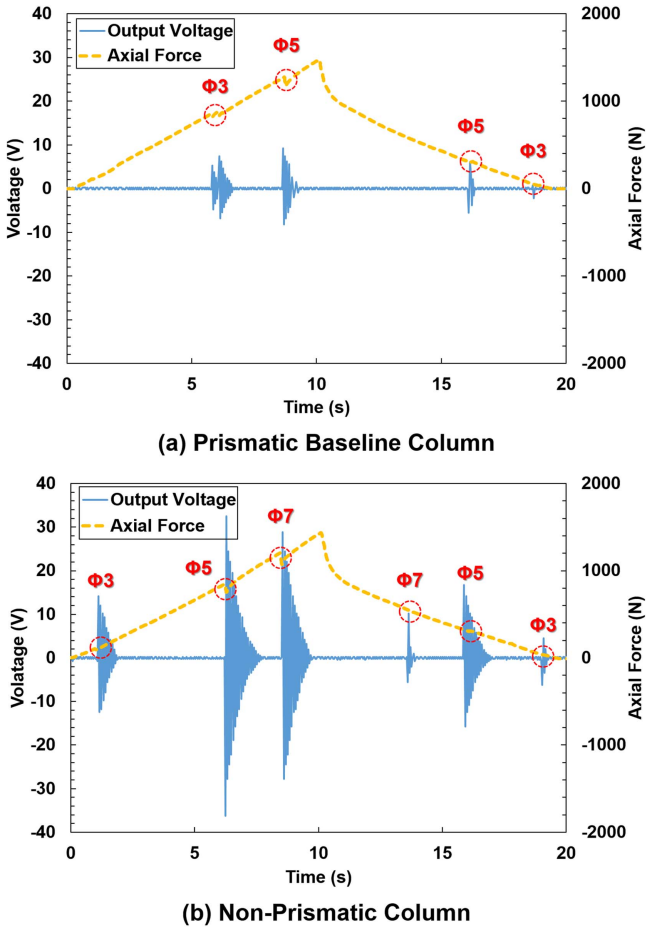

Figure 13. Piezoelectric output voltage generated for (a) prismatic baseline column and (b) non-prismatic column with $\alpha = 0.80/\beta = 0.40$.

5. Conclusions

This paper presented numerical and experimental studies to demonstrate how the buckling location of multiple mode transitions in bilaterally constrained columns under compression can be controlled by introducing flexural stiffness variations along the column length. A theoretical model was developed based on the stationary potential energy principle through a simplified approach for predicting the growth of the critical line contact segment length and the column's buckling morphologies as axial compression proceeds. Non-prismatic designs (obtained through thickness variations in discrete form along the column length) increase local instabilities in the elastic postbuckling regime, which increases the number of buckling mode transitions compared to prismatic columns for the same global strain level. Results show that increased stiffness regions in non-prismatic columns are able to define where local buckling will be triggered, such that columns with stiffness variations within an identified design domain can attain a controllable location for the buckling events. Therefore, a predefined high kinetic energy release spot can be designed on the strip. This feature allows predicting where buckling will occur so that piezoelectric oscillators can be optimally placed on the strip for use in energy harvesting

devices. The direct relation between the acceleration base input and the voltage output of piezoelectric oscillator transducers allows the tailorable postbuckling response features of non-prismatic columns to be used as a multi-stable energy concentrator strip with enhanced performance, in terms of more sustainable voltage output from mounted piezoelectric oscillators, for use in quasi-static micro-energy harvesting devices.

Acknowledgments

The presented work was carried out with support from the US National Science Foundation under grant number ECCS-1408506. The authors gratefully acknowledge the technical support of Mr Mingzhe Li (MSU) on the experimental testing, Dr Junfeng Xiao (Columbia University) on the theoretical model, and Mr Brian Wright (MSU) on specimen manufacturing.

References

[1] Hu N 2015 Buckling-induced smart applications: recent advances and trends *Smart Mater. Struct.* **24** 063001
[2] Reis P M 2015 A perspective on the revival of structural (In) stability with novel opportunities for function: from Buckliphobia to Buckliphilia *J. Appl. Mech.* **82** 111001
[3] Stephen N 2006 On energy harvesting from ambient vibration *J. Sound Vib.* **293** 409–25
[4] Sodano H A, Inman D J and Park G 2004 A review of power harvesting from vibration using piezoelectric materials *Shock Vib. Dig.* **36** 197–206
[5] Park G *et al* 2008 Energy harvesting for structural health monitoring sensor networks *J. Infrastruct. Syst.* **14** 64–79
[6] Mann B and Sims N 2009 Energy harvesting from the nonlinear oscillations of magnetic levitation *J. Sound Vib.* **319** 515–30
[7] Harne R and Wang K 2013 A review of the recent research on vibration energy harvesting via bistable systems *Smart Mater. Struct.* **22** 023001
[8] Jung S-M and Yun K-S 2010 Energy-harvesting device with mechanical frequency-up conversion mechanism for increased power efficiency and wideband operation *Appl. Phys. Lett.* **96** 111906
[9] Sneller A, Cette P and Mann B 2011 Experimental investigation of a post-buckled piezoelectric beam with an attached central mass used to harvest energy *Proc. Inst. Mech. Eng.* I **225** 497–509
[10] Cottone F *et al* 2012 Piezoelectric buckled beams for random vibration energy harvesting *Smart Mater. Struct.* **21** 035021
[11] Van Blarigan L, Danzl P and Moehlis J 2012 A broadband vibrational energy harvester *Appl. Phys. Lett.* **100** 253904
[12] Xiong L, Tang L and Mace B R 2016 Internal resonance with commensurability induced by an auxiliary oscillator for broadband energy harvesting *Appl. Phys. Lett.* **108** 203901
[13] Erturk A and Inman D 2011 Broadband piezoelectric power generation on high-energy orbits of the bistable Duffing oscillator with electromechanical coupling *J. Sound Vib.* **330** 2339–53
[14] Peters C *et al* 2008 Novel electrically tunable mechanical resonator for energy harvesting *Proc. PowerMEMS 2008* pp 253–6
[15] Soliman M *et al* 2008 A wideband vibration-based energy harvester *J. Micromech. Microeng.* **18** 115021
[16] Kim H S, Kim J-H and Kim J 2011 A review of piezoelectric energy harvesting based on vibration *Int. J. Precis. Eng. Manuf.* **12** 1129–41
[17] Chai H 1998 The post-buckling response of a bi-laterally constrained column *J. Mech. Phys. Solids* **46** 1155–81
[18] Chai H 2002 On the post-buckling behavior of bilaterally constrained plates *Int. J. Solids Struct.* **39** 2911–26
[19] Stein E, Wagner W and Wriggers P 1990 Nonlinear stability-analysis of shell and contact-problems including branch-switching *Comput. Mech.* **5** 428–46
[20] Lajnef N *et al* 2014 A concept for energy harvesting from quasi-static structural deformations through axially loaded bilaterally constrained columns with multiple bifurcation points *Smart Mater. Struct.* **23** 055005
[21] Xiao J and Chen X 2013 Buckling morphology of an elastic beam between two parallel lateral constraints: implication for a snake crawling between walls *J. R. Soc. Interface* **10** 20130399
[22] Roman B and Pocheau A 2002 Postbuckling of bilaterally constrained rectangular thin plates *J. Mech. Phys. Solids* **50** 2379–401
[23] Timoshenko S P and Gere J M 2009 *Theory of Elastic Stability* 2nd edn (Minneola, NY: Dover)
[24] Plaut R H and Yang Y-W 1995 Behavior of three-span braced columns with equal or unequal spans *J. Struct. Eng.* **121** 986–94
[25] Javaheri R and Eslami M 2002 Buckling of functionally graded plates under in-plane compressive loading *ZAMM—J. Appl. Math. and Mech./(Z. Angew. Math. Mech.)* **82** 277–83
[26] Dinnik A 1929 Design of columns of varying cross section *Trans. ASME* **51** 105–14
[27] Timoshenko S 1908 *Buckling of Bars of Variable Cross Section* (Kiev, USSR: Bulletin of the Polytechnic Institute)
[28] Elishakoff I 2000 Both static deflection and vibration mode of uniform beam can serve as a buckling mode of a non-uniform column *J. Sound Vib.* **232** 477–89
[29] Elishakoff I 2004 *Eigenvalues of Inhomogeneous Structures: Unusual Closed-Form Solutions* (Boca Raton, FL: CRC Press)
[30] Arbabi F and Li F 1991 Buckling of variable cross-section columns: integral-equation approach *J. Struct. Eng.* **117** 2426–41
[31] Wang C and Wang C Y 2004 *Exact Solutions for Buckling of Structural Members* vol 6 (Boca Raton, FL: CRC press)
[32] Pasini D 2007 Shape transformers for material and shape selection of lightweight beams *Mater. Des.* **28** 2071–9
[33] Pasini D 2006 Shape and material selection for optimizing flexural vibrations in multilayered resonators *J. Microelectromech. Syst.* **15** 1745–58
[34] Hu N and Burgueño R 2015 Tailoring the elastic postbuckling response of cylindrical shells: a route for exploiting instabilities in materials and mechanical systems *Extreme Mech. Lett.* **4** 103–10
[35] Elvin N G and Elvin A A 2009 A general equivalent circuit model for piezoelectric generators *J. Intell. Mater. Syst. Struct.* **20** 3–9
[36] Lazarus A and Reis P M 2015 Soft actuation of structured cylinders through auxetic behavior *Adv. Eng. Mater.* **17** 815–20